Identification of Electrical Appliances via Analysis of Power Consumption

Roman Streubel and Bin Yang
Institute for Signal Processing and System Theory
University of Stuttgart
Email: rom@nstreubel.de and bin.yang@iss.uni-stuttgart.de

***Abstract*—Identification of small electrical appliances via power consumption requires accurate detection and evaluation of steady-state sections and transient sections. However, the steady-state sections and transient sections are extracted from low frequency sampled (1 Hz) power measurements. We gain the steady-state sections and transient sections by processing real and reactive power measurements with a robust bucketing technique and unsupervised clustering. Macroscopic features for detected steady-state sections and transient sections are then extracted. Besides, our method estimates the similarity of steady-state sections and transient sections and determines recurred sections accurately. The proposed method is applicable for an inexpensive, unsupervised learning of small electrical appliances in real time.**

***Index Terms*—Nonintrusive Appliance Load Monitoring, Finite State Machine, Bucketing Technique, Unsupervised Clustering, Transient Detection, Adjacency Matrix**

I. Introduction

Efficient energy use becomes more and more important for industrial environment as well as for private households. In order to enable energy management systems, two approaches for monitoring energy are known. Intrusive load monitoring and nonintrusive load monitoring (NILM). Monitoring energy consumption in an intrusive way has the disadvantage that in so called home automation networks a two-way communication is required for *each* electrical appliance. Hence, the intrusive load monitoring procedure is costly since only expensive and/or novel devices like washing machines or refrigerators are optionally equipped with network interfaces. Upgrading each old or low cost device with an additional network interface in a private household is too expensive. In case of NILM, the individual appliance power consumption information is disaggregated from a single meter and does not require any upgrades on existing household appliances which is the big advantage of NILM. NILM is separated into two different approaches in terms of the sampling frequency f_s. Power consumption signatures obtained with high sampling frequency $f_s \geq 8$ kHz are called microscopic features and features which are gained by a low sampling frequency $f_s \leq 1$ Hz are called macroscopic features [1]. Whereas microscopic features might help to monitor continuously variable devices via observation of transients, they are far too expensive for on-off or simple finite state machine (FSM) devices. Accurate steady-state and transient detection as well as recognition of recurrent sections are mandatory for the identification of electrical appliances, especially in terms of NILM with a low sampling frequency.

In the present contribution we denoise the given signal by assuming signal dependent and Poisson distributed noise and estimate the model order M via a robust bucketing technique in the noiseless $\overline{PQ}$-plane. Followed by detection of the steady-state sections Π and transient sections Ψ via unsupervised clustering with expectation maximization (EM) algorithm and Gaussian mixture model (GMM) of the unfiltered raw signal. Macroscopic features for detected steady-state sections Π and transient sections Ψ are computed including apparent power S, real power P and reactive power Q. Observations have shown that desired information about characteristic peaks of transients get lost if measurement signals are low-pass or median filtered. Hence, in our proposed algorithm no low-pass or median filtering at physical measurements is applied directly. Besides, our method determines recurred sections via similarity estimation for detected steady-state sections Π and transient sections Ψ.

II. Related Work

Current research focuses on different areas for NILM in industrial buildings or private residences (households). Algorithms with NILM have mostly three limiting assumptions. Loads are distinguishable, have steady-states and are batch processed [2]. According to [3], another issue is that most NILM algorithms process data in batch format using a day or more which is not even close to real-time requirement. Reference [4] proposed a method consisting of fuzzy clustering combined with genetic algorithms and a dynamic programming algorithm. They considered only changes of real power P and concluded that typical patterns of on-off appliances or FSMs with less than five different steady-states were detected without any a priori knowledge. Worth remarking is that the same author used in Ref. [5] a nonlinear and dynamically adapted threshold, while in Ref. [4] the dynamic threshold was replaced by a fixed threshold. Rare and small events were neglected in this approach. Reference [6] extended the work of the well known Ref. [7] by applying a median filter to remove outlier in the signal. Reference [2] proposed two approaches, a heuristic approach and a Bayesian approach. The proposed algorithms started with interpolation and filtering of real power P and reactive power Q before applying an edge detection. They considered changes in

both real power P and reactive power Q equally. Reference [8] concluded that steady-states can not serve as a reliable load discriminator if several devices are active and that only transients, and slopes are unique features to distinguish loads. Hence, steady-states were neglected. Reference [6] concluded that recurrence of transients is poor in energy consumption of industrial buildings.

The main difference to other methods is the procedure to detect transients in given signals. Common are edge detection algorithms. Edge detection algorithms with pre-filtering have the disadvantage to provide just a single point of occurrence in time and not the complete transient sections Ψ with all characteristic spikes. In contrast we use each raw unfiltered sample to retrieve as much information as possible and assume that only one device at a time is active in order to detect steady-states and transients properly. Furthermore, we weight measured real power P and reactive power Q values in our algorithm differently and show that recurrent steady-states and transients are detectable in case of small appliances.

III. FSM Model and Test Sequence

Figure 1 shows a general FSM model. The FSM model defines the steady-states from η_{O}, η_{A}, ... to $\eta_{\dots}$ as well as the transients ξ_{OA}, ξ_{AA}, ... to $\xi_{\dots}$. Please note, we introduce additional transitions during the steady-states. The reason for this will become clear in Section IV. In this FSM model, a simple on-off device consists of two steady-states η_{O} and η_{A} and three transients ξ_{OA}, ξ_{AA} and ξ_{AO} where η_{O} is an inactive device state. A FSM device with four modes of operation consists of four steady-states η_{O}, η_{A}, η_{B} and η_{C} and fifteen transients (solid and dashed lines) where again η_{O} is an inactive device state.

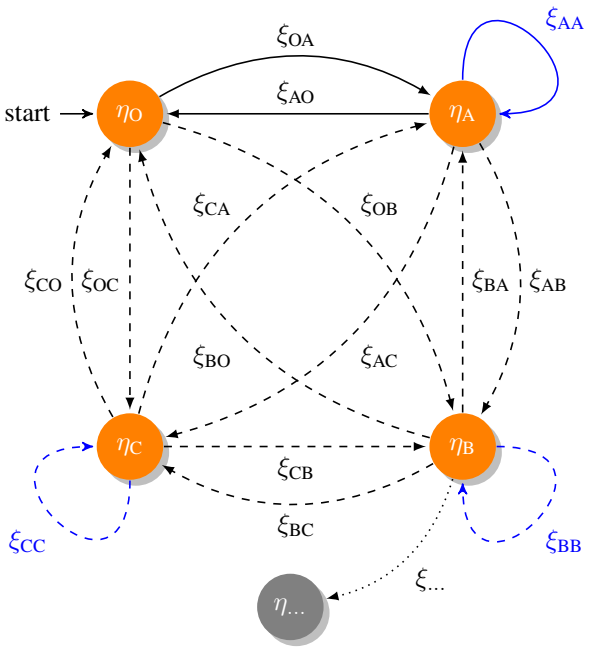

Fig. 1. A general FSM model for devices with several modes of operation.

Figure 2 shows the test sequence of power consumption measurements used in this paper. The sequence starts with an active standing fan (SF) and inactive compact fluorescent lamp (CFL) and continues with CFL as active and SF as inactive. Therefore, *only one device at a time is active*. The SF has in this case four modes of operation and the CFL has two. The inactive device states are replaced with one off-state. The given sequence is actually a concatenation of two single physical measurements. The challenge is to detect all single and recurrent sections.

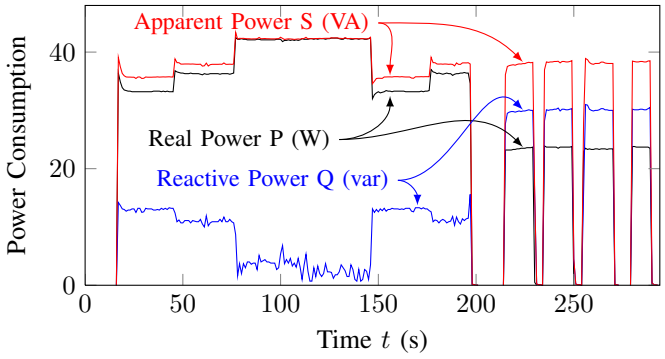

Fig. 2. Apparent power S with real power P and reactive power Q of a SF with four modes of operation and the same measurement of a CFL with two modes of operation afterwards. The SF is active from $t = 16$ s to $t = 201$ s and shows three different active states. The CFL is active from $t = 214$ s to $t = 294$ s and is switched on-off four times.

IV. Unsupervised Clustering

To be able to monitor electrical appliances nonintrusively, unsupervised clustering in the $\overline{PQ}$-plane is desired. Let M be the true number of clusters and $\tilde{M}$ be the estimated one. If $\tilde{M} < M$, two ore more steady-state clusters will be detected as one and we will miss the transients between steady-state sections. If $\tilde{M} > M$, one or more steady-state clusters are divided into several clusters and transients between such divided steady-state clusters occur additionally. Since we tolerate additional transients during steady-states (see Fig. 1), the overestimated case is more acceptable than the underestimated case which has to be avoided. Therefore the estimation of model order M is mandatory before applying a clustering method to the data. For simplification, we make the following assumptions. A steady-state must be *active* for a minimum time of $\check{t}_{\Pi} = 3$ s. The transient duration t^{Ψ} is *not* limited. We also assume that the steady-states represented as clusters in $\overline{PQ}$-plane are *Gaussian* distributed and state dependent. Additionally, all other occurring values outside of the clusters in the $\overline{PQ}$-plane are assumed to be Poisson distributed noise which is signal dependent. Due to the assumption of Gaussian distributed clusters in the raw $\overline{PQ}$-plane, we apply the EM algorithm to estimate the underlying GMM from the real power P and reactive power Q measurements. Before doing that, we first apply the bucketing technique to estimate model order M, the number of clusters for steady-states.

Figure 3 illustrates the complex power $\overline{PQ}$-plane for the measurement in Fig. 2. We see clearly five clusters represented by the red samples and five detected steady-state clusters. Additional noise is present as well as values which represent transients.

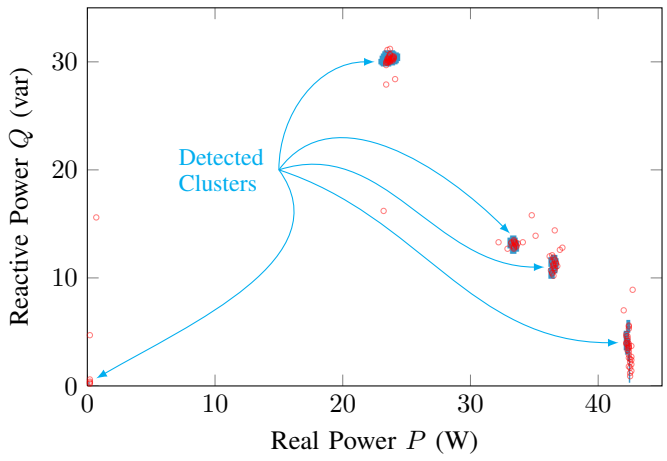

Fig. 3. Complex power plane $\overline{PQ}$ for the measurement in Fig. 2 and five detected steady-state clusters.

A. Model Order Estimation

As a first step, we apply a bucketing technique which is known from image processing. Each sample of real power P and reactive power Q is binned into a container with bin size of 0.1 in each dimension in the $\overline{PQ}$-Plane. Each incoming sample in a container is considered as an increasing intensity level of a pixel in an image $\mathcal{I}_a$. The intensity level per pixel is represented in the following with occurence value κ. The bucketing technique simply creates a two-dimensional histogram with a constant bin size.

Figure 4(a) illustrates the created two-dimensional histogram of a $\overline{PQ}$-plane section as an image $\mathcal{I}_a$. We use the Moore-Neighbor tracing algorithm with Jacob's stopping criterion to obtain single pixels and objects out of image $\mathcal{I}_a$.

Figure 4(b) with image $\mathcal{I}_b$ contains the separated objects and image $\mathcal{I}_c$ in Fig. 4(c) the extracted single pixels. The single pixels in image $\mathcal{I}_c$ are thresholded in the next step. Due to the assumption of Poisson distributed noise we can filter the single pixels in image $\mathcal{I}_c$ via consideration of its respective occurrence value κ and separate them into sample of a cluster or sample of a transient. Therefore we seek a threshold τ for the case that more than κ samples fall into one container with the probability $p \leq 0.1\%$. In order to be able to compute the threshold τ we collect all pixels with occurrence $\kappa = 0$ in image $\mathcal{I}_a$ and all single pixels with occurrence $\kappa > 0$ in $\mathcal{I}_c$ into one single pixel vector f. Then we estimate with single pixel vector f the sample mean

$$\hat{\lambda} = \frac{1}{N_f} \sum_{n=1}^{N_f} f(n) \tag{1}$$

with the number of elements N_f in f and compute the threshold τ via

$$\sum_{k=0}^{\tau} \left[P(k=\tau) = \frac{\hat{\lambda}^k e^{-\hat{\lambda}}}{k!} \right] > 0.999. \tag{2}$$

Single pixels in image $\mathcal{I}_c$ with occurrence $\kappa \leq \tau$ are neglected and only single pixels with occurrence $\kappa > \tau$ are transferred together with the objects from image $\mathcal{I}_b$ into image $\mathcal{I}_d$ in Fig. 4(d) for further processing.

Since we assume that the pixels in image $\mathcal{I}_d$ represent samples of clusters only and that occurring clusters in $\overline{PQ}$-plane are also signal dependent, the idea is now to model the uncertainty for *each* given pixel in image $\mathcal{I}_d$. The image $\mathcal{I}_d$ is converted into a binary image $\mathcal{I}_e$ illustrated in Fig. 4(e). Now we introduce measurement error factors e_P and e_Q which depend on the accuracy of the used measurement device. The first variable ellipse radius

$$r_a = e_Q Q(n) \tag{3}$$

is depending on reactive power Q and the respective measurement error factor e_Q. The second variable ellipse radius

$$r_b = e_P P(n) \tag{4}$$

is related to real power P and the respective measurement error factor e_P. Both constant error factors $e_P = 0.011$ and $e_Q = 0.015$ were adjusted empirically and work with container bin size of 0.1. The idea is to "stamp" a filled ellipse

$$(P - P(n))^2/r_a^2 + (Q - Q(n))^2/r_b^2 = 1 \tag{5}$$

of variable size depending on each pixel in the binary image $\mathcal{I}_e$ where $P(n)$ and $Q(n)$ are the ellipse center. The result in Fig. 4(f) is achieved via binary cross correlation including binary image $\mathcal{I}_e$ and each variable ellipse. The final objects in image $\mathcal{I}_f$ are again obtained via Moore-Neighbor tracing algorithm. The number of objects and single pixels in image $\mathcal{I}_f$ equals the estimated model order $\tilde{M}$. Important to note is that we increment the estimated model order $\tilde{M}+1$ in the case that single pixels with occurrence κ below the threshold τ were neglected. This step is applied because of the fact that the bucketing method estimates the model order in an almost completely noise free image $\mathcal{I}_f$. In order to apply the estimated model order $\tilde{M}$ correctly on a noisy raw $\overline{PQ}$-plane the incrementation step is necessary to have an additional cluster index for classification of noise only.

B. Gaussian Mixture Model Estimation via Expectation-Maximization

Since the initial parameters for the estimation are set randomly we apply the EM algorithm ten times on the raw $\overline{PQ}$-plane. The final GMM is the estimated one with the lowest negative log likelihood value for the corresponding parameters. We obtain as a result with the final GMM the cluster index vector $v \in \mathbb{N}^N$ which contains cluster indices $c \in \{1, \ldots, \tilde{M}\}$ where N is the number of samples per physical measurement. We used the EM algorithm which is implemented in the MATLAB function `gmdistribution.fit`.

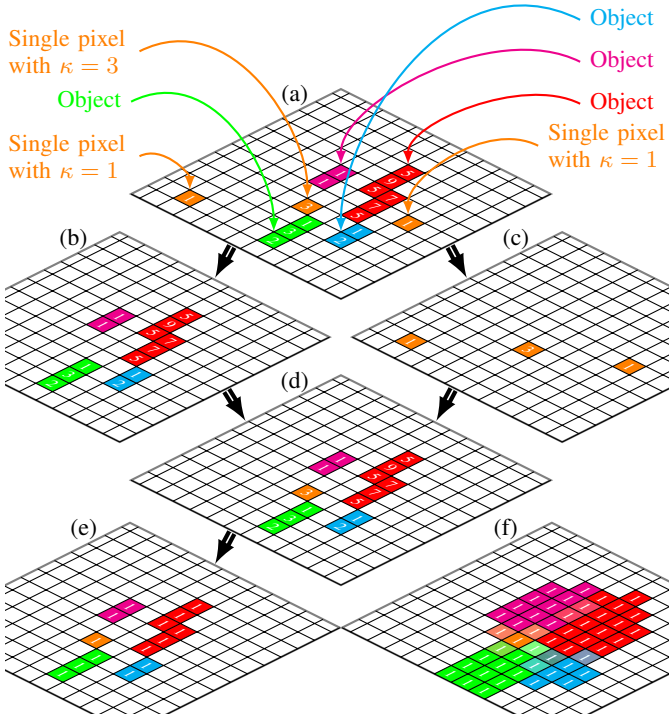

Fig. 4. Algorithm procedure for applied bucketing technique on (a) segment out of $\overline{PQ}$-plane as an image $\mathcal{I}_a$ and definition of objects and single pixels; (b) extraction of objects onto image $\mathcal{I}_b$; (c) extraction of single pixels onto image $\mathcal{I}_c$ and further observation on selected single pixels to detect representations of clusters; (d) combination of already selected objects and outcome of single pixel observation as additional objects onto image $\mathcal{I}_d$; (e) followed by conversion to a binary image $\mathcal{I}_e$; (f) outcome of binary cross correlation with each variable ellipse depending on measurement errors e_P and e_Q.

V. State Detection

The cluster index c for each detected cluster in the cluster index vector $v(n)$ changes mostly since the initial parameters in EM algorithm are generated randomly. Hence we consider the absolute second order difference vector $w(n) = |v(n)''|$ of v. The the absolute second order difference vector $w(n)$ is used to suppress detection of maxima or minima points. In general, a single zero in $w(n)$ represents *only* a turning point in the cluster index vector v. The binary state vector

$$m(n) = \begin{cases} 1, & w(n) = 0, \\ 0, & w(n) > 0 \end{cases} \qquad 1 \le n \le N \tag{6}$$

indicates steady-state sections Π where $m(n) = 1$ and transient sections Ψ where $m(n) = 0$. The binary state vector m consists of N elements which is the number of samples in one measurement. In order to suppress detection of turning points as steady-state sections and to ensure our constraint of minimum steady-state duration of $\check{t}_\Pi = 3$ s, we simply remove such single ones in $m(n)$ without loss of information: $(\ldots, 0, 1, 0, \ldots) \mapsto (\ldots, 0, 0, 0, \ldots)$.

In the final binary state vector m, each consecutive sequence of ones represents a steady-state section Π_i with $1 \le i \le n_\Pi$ where n_Π is the number of detected steady-state sections. Each consecutive sequence of zeros represents a transient section Ψ_j with $1 \le j \le n_\Psi$ where n_Ψ is the number of detected transient sections. The sections are extracted out of the given power measurement with the binary state vector m as a mask.

Figure 5 illustrates the obtained steady-state sections Π and transient sections Ψ for our given test sequence of apparent power measurement. This result is achieved via our model order estimation method, followed by EM algorithm with GMM and our state detection. Steady-state sections Π are plotted in red and labelled from section Π_1 to Π_{15}. Transient sections Ψ are plotted in blue and labelled from section Ψ_1 to Ψ_{14}. Clearly visible are the well preserved characteristic spikes in the transient sections and the accurately detected steady-state sections.

VI. Macroscopic Features

After accurate and robust detection of steady-state and transient sections, respective feature computation is necessary to be able to classify each detected section properly. In the following we make the assumption that steady-state sections Π are characterized by linear and transient sections Ψ by nonlinear behaviour. The feature computation is done for *each* section separately with its respective apparent power S, real power P and reactive power Q measurements where n_Π is the number of detected steady-state sections Π and n_Ψ is the number of detected transient sections Ψ. For simplicity we use the notation $X \in \{S, P, Q\}$ in the following to denote apparent, real and reactive power measurements.

A. Steady-State Section Features

The features for *each* steady-state section Π_i with $1 \le i \le n_\Pi$ are computed as follows. The mean value

$$\bar{\Pi}_i^X = \frac{1}{N_i^\Pi} \sum_{n=0}^{N_i^\Pi - 1} \Pi_i^X(n) \tag{7}$$

is used to compute the down shifted steady-state section

$$\check{\Pi}_i^X(n) = \Pi_i^X(n) - \bar{\Pi}_i^X \qquad 0 \le n \le N_i^\Pi - 1 \tag{8}$$

where N_i^Π is the number of samples per steady-state section Π_i. The down shifted steady-state section $\check{\Pi}_i^X$ is then estimated by a first order robust regression

$$\check{\Pi}_i^X(n) \approx \alpha_i^X n + \beta_i^X \qquad 0 \le n \le N_i^\Pi - 1 \tag{9}$$

using bisquare weights and its respective first coefficient α_i^X and second coefficient β_i^X. The usage of robust fit algorithm is more solid against single outliers and provides more constant estimates compared to a least square method which is sensitive to outliers.

The resulting temporary feature vector

$$x_i^X = \left(\alpha_i^X, \beta_i^X, \bar{\Pi}_i^X, \tilde{\Pi}_i^X, [(\bar{\Pi}_i^X < 2)?], \sigma_i^X\right)_{1\times 6} \tag{10}$$

consists additional of the logic value $[(\bar{\Pi}_i^X < 2)?]$, median value $\tilde{\Pi}_i^X$ of the down shifted steady-state section $\check{\Pi}_i^X$ and the

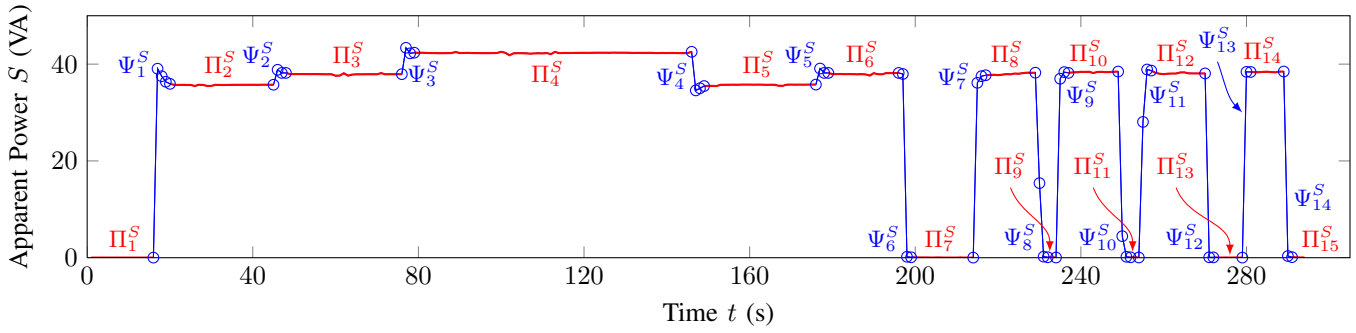

Fig. 5. The apparent power measurement is masked and labelled by our state detection algorithm. Clearly visible are the well preserved characteristic spikes in the transient sections Ψ and the accurately detected steady-state sections Π.

respective variance σ_i^X. The logic value $[(\bar{\Pi}_i^X < 2)?]$ is used to identify if a steady-state section Π_i represents an inactive steady-state or an active steady-state. All temporary feature vectors x_i^X are then concatenated to form the final steady-state feature vector $g_i^\Pi = (x_i^S\, x_i^P\, x_i^Q)$. Overall, each steady-state feature vector $g_i^\Pi \in \mathbb{R}^{d_\Pi}$ has $d_\Pi = 18$ dimensions.

B. Transient Section Features

The features for *each* transient section Ψ_j with $1 \leq j \leq n_\Psi$ are computed as follows. The minimum value

$$\check{\Psi}_j^X = \min_n \left[\Psi_j^X(n)\right] \qquad 0 \leq n \leq N_j^\Psi - 1 \tag{11}$$

is used to compute down shifted transient section

$$\mathring{\Psi}_j^X(n) = \Psi_j^X(n) - \check{\Psi}_j^X \qquad 0 \leq n \leq N_j^\Psi - 1. \tag{12}$$

The down shifted transient section $\mathring{\Psi}_j^X$ is then estimated by a sixth order least squares fit

$$\begin{aligned}\mathring{\Psi}_j^X(n) \approx\ & \alpha_j^X n^6 + \beta_j^X n^5 + \gamma_j^X n^4 + \delta_j^X n^3 \\ & + \epsilon_j^X n^2 + \varepsilon_j^X n + \zeta_j^X \qquad 0 \leq n \leq N_j^\Psi - 1\end{aligned} \tag{13}$$

with its respective first coefficient α_j^X up to seventh coefficient ζ_j^X. The sixth order least squares fit is necessary to retrieve accurate estimations of occurring turn-on and turn-off transient with all characteristic positive and negative spikes. Gradients of transient sections Ψ are also very characteristic. Therefore the maximum gradient value $\max_n[(\mathring{\Psi}_j^X)']$ and the minimum gradient value $\min_n[(\mathring{\Psi}_j^X)']$ of the approximated slope $(\mathring{\Psi}_j^X)'$ are also used as features. Further feature is the delta value

$$\Delta\mathring{\Psi}_j^X = \mathring{\Psi}_j^X(N_j^\Psi - 1) - \mathring{\Psi}_j^X(0). \tag{14}$$

The resulting temporary feature vector

$$\begin{aligned}x_j^X = \Bigg(&\alpha_j^X, \beta_j^X, \gamma_j^X, \delta_j^X, \epsilon_j^X, \varepsilon_j^X, \zeta_j^X, \max_n\left[\left(\mathring{\Psi}_j^X\right)'\right], \\ &\min_n\left[\left(\mathring{\Psi}_j^X\right)'\right], \Delta\mathring{\Psi}_j^X, \hat{t}_j^X, \check{t}_j^X, \mathring{t}_j^X\Bigg)_{1\times 13}\end{aligned} \tag{15}$$

consists additional of discrete rise time $\hat{t}_j^X$ where the approximated slope $(\mathring{\Psi}_j^X)'$ is positive, discrete fall time $\check{t}_j^X$ where the approximated slope $(\mathring{\Psi}_j^X)'$ is negative and the discrete constant time $\mathring{t}_j^X$ where the approximated slope $(\mathring{\Psi}_j^X)'$ is zero. The time values are given in seconds. All temporary feature vectors x_j^X are then concatenated to form the final transient feature vector $g_j^\Psi = (x_j^S\, x_j^P\, x_j^Q)$. Overall, each transient feature vector $g_j^\Psi \in \mathbb{R}^{d_\Psi}$ has $d_\Psi = 39$ dimensions.

VII. Similarity Estimation

So far, steady-state sections Π and transient sections Ψ are detected and respective feature vectors g^Π and g^Ψ are computed. The challenge is now to detect recurrences of steady-state and transient sections to allow collecting more information about repeated steady-states or transients in the measurement. For simplicity, we use the generic notation $X \in \{\Pi, \Psi\}$ in the following to denote a steady or transient state. Please note, the norm of each feature vector g^X is normalized to one.

We compare three commonly used distance metrics for estimating similarity of feature vectors: the well known Euclidean distance matrix

$$E_X(i,j) = \|g_i^X - g_j^X\| \qquad 1 \leq i,j \leq n_X, \tag{16}$$

the city block distance matrix

$$B_X(i,j) = \sum_{n=1}^{d_X} |g_i^X(n) - g_j^X(n)| \tag{17}$$

and the correlation distance matrix

$$C_X(i,j) = 1 - (g_i^X - \overline{g}_i^X)(g_j^X - \overline{g}_j^X)^{\mathrm{T}} / z_{i,j}^X \tag{18}$$

with mean $\overline{g}_i^X = 1/d_X \sum_{n=1}^{d_X} g_i^X(n)$, $\overline{g}_j^X = 1/d_X \sum_{n=1}^{d_X} g_j^X(n)$ and $z_{i,j}^X = \|g_i^X - \overline{g}_i^X\|\|g_j^X - \overline{g}_j^X)\|$.

Figure 6(a) shows the different distance metrics for steady-state section Π_6 with the feature vector g_6^Π as reference. It is known that both steady-state sections Π_3 and Π_6 represent the same steady-state. The city block metric has the advantage that the distance values are bigger compared to the correlation and Euclidean metric at distances to feature vectors g_2^Π, g_4^Π and g_5^Π. Additionally the distance to the feature vectors g_8^Π, g_{10}^Π, g_{12}^Π, and g_{14}^Π is largest. Figure 6(b) plots the different distance metrics for transient section Π_7 with the feature

vector g_7^{Π} as reference. In this case, it is known that transient sections Ψ_7, Ψ_9, Ψ_{11}, and Ψ_{13} represent the same transient. Here, the correlation metric is preferred because the feature vectors g_7^{Ψ}, g_9^{Ψ}, g_{11}^{Ψ}, and g_{13}^{Ψ} lie closer together compared to city block and Euclidean distance. Furthermore the feature vector g_1^{Ψ} is also still separable from feature vector g_7^{Ψ}.

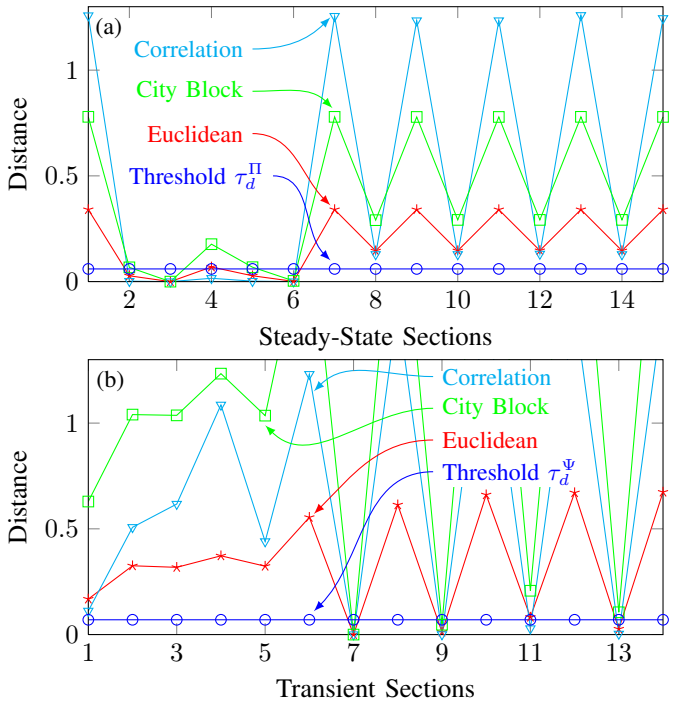

Fig. 6. (a) Distance of the steady-state feature vector g_6^{Π} to all other steady-state feature vectors. Both steady-state feature vectors g_3^{Π} and g_6^{Π} represent the same steady-state. (b) Distance of the transient feature vector g_7^{Ψ} to all other transient feature vector. The transient feature vectors g_7^{Ψ}, g_9^{Ψ}, g_{11}^{Ψ}, and g_{13}^{Ψ} represent the same transient.

Therefore, in order to determine recurrences we propose the symmetric adjacency matrix

$$A_{\Pi}(i,j) = \begin{cases} 1, & B_{\Pi}(i,j) \leq \tau_d^{\Pi}, \\ 0, & \text{otherwise} \end{cases} \qquad 1 \leq i,j \leq n_{\Pi} \tag{19}$$

for steady-state sections with the distance threshold τ_d^{Π}. For transient sections, the symmetric adjacency matrix

$$A_{\Psi}(i,j) = \begin{cases} 1, & C_{\Psi}(i,j) \leq \tau_d^{\Psi}, \\ 0, & \text{otherwise} \end{cases} \qquad 1 \leq i,j \leq n_{\Psi} \tag{20}$$

is obtained by comparing the correlation distance matrix C_{Ψ} to the distance threshold τ_d^{Ψ}. In this paper, the distance thresholds are $\tau_d^{\Pi} = 0.06$ and $\tau_d^{\Psi} = 0.07$.

Figure 7(a) illustrates the detected recurrences of steady-state sections from the adjacency matrix A_{Π}. *All* single and recurrent steady-states are detected correctly. Figure 7(b) shows the detected recurrences of transient sections from the adjacency matrix A_{Ψ}. *All* single and recurrent transients are detected correctly as well.

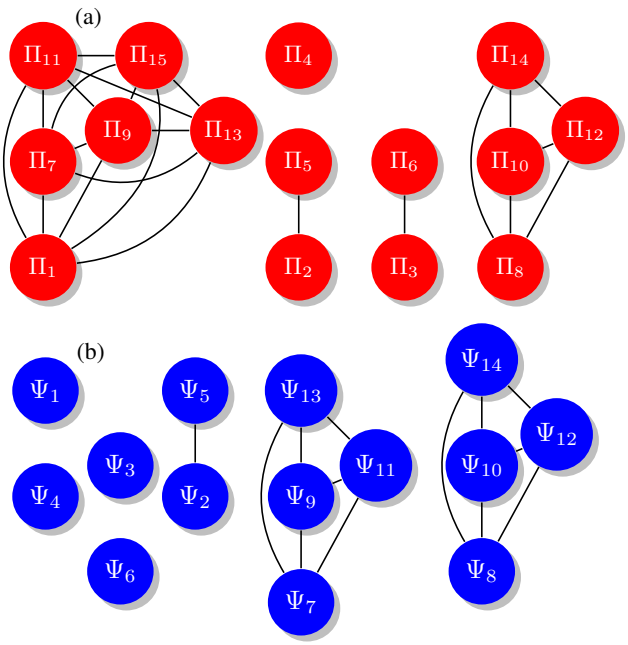

Fig. 7. (a),(b) Resulting graphs in adjacency matrix A_{Π} and A_{Ψ}. Each connected graph indicates the detected recurrences of steady-state or transient sections. A single node represents an one-time only section. Here, all recurrence detections are correct for the test sequence.

VIII. Conclusion

We developed an unsupervised, fast, robust and inexpensive algorithm to disaggregate steady-state and transient sections accurately from low sampling frequency power measurements. The algorithm was tested on a power measurement sequence consisting of a standing fan (SF) and a compact fluorescent lamp (CFL). All different steady-state and transient sections of both devices are detected correctly. In addition, we can also correctly detect the recurrence of the same device states and transients.

References

[1] M. Zeifman and K. Roth, "Nonintrusive appliance load monitoring: Review and outlook," *Consumer Electronics, IEEE Transactions on*, vol. 57, no. 1, pp. 76–84, 2011.

[2] A. Marchiori, D. Hakkarinen, Q. Han, and L. Earle, "Circuit-level load monitoring for household energy management," *Pervasive Computing, IEEE*, vol. 10, no. 1, pp. 40–48, 2011.

[3] C. Laughman, K. Lee, R. Cox, S. Shaw, S. Leeb, L. Norford, and P. Armstrong, "Power signature analysis," *Power and Energy Magazine, IEEE*, vol. 1, no. 2, pp. 56–63, 2003.

[4] M. Baranski and J. Voss, "Genetic algorithm for pattern detection in nialm systems," in *Systems, Man and Cybernetics, 2004 IEEE International Conference on*, vol. 4, 2004, pp. 3462–3468.

[5] ——, "Nonintrusive appliance load monitoring based on an optical sensor," in *Power Tech Conference Proceedings, 2003 IEEE Bologna*, vol. 4, 2003, p. 8 pp.

[6] L. K. Norford and S. B. Leeb, "Non-intrusive electrical load monitoring in commercial buildings based on steady-state and transient load-detection algorithms," *Energy and Buildings*, vol. 24, no. 1, pp. 51–64, 1996.

[7] G. Hart, "Nonintrusive appliance load monitoring," *Proceedings of the IEEE*, vol. 80, no. 12, pp. 1870–1891, 1992.

[8] A. Cole and A. Albicki, "Data extraction for effective non-intrusive identification of residential power loads," in *Instrumentation and Measurement Technology Conference, 1998. IMTC/98. Conference Proceedings. IEEE*, vol. 2, 1998, pp. 812–815.